Adaptive conductance filtering for spatially varying noise in PET images

Dirk Ryan Padfield and Ravindra Manjeshwar

GE Global Research, Niskayuna, NY, 12309, USA

ABSTRACT

PET images that have been reconstructed with unregularized algorithms are commonly smoothed with linear Gaussian filters to control noise. Since these filters are spatially invariant, they degrade feature contrast in the image, compromising lesion detectability. Edge-preserving smoothing filters can differentially preserve edges and features while smoothing noise. These filters assume spatially uniform noise models. However, the noise in PET images is spatially variant, approximately following a Poisson behavior. Therefore, different regions of a PET image need smoothing by different amounts. In this work, we introduce an adaptive filter, based on anisotropic diffusion, designed specifically to overcome this problem. In this algorithm, the diffusion is varied according to a local estimate of the noise using either the local median or the grayscale image opening to weight the conductance parameter. The algorithm is thus tailored to the task of smoothing PET images, or any image with Poisson-like noise characteristics, by adapting itself to varying noise while preserving significant features in the image. This filter was compared with Gaussian smoothing and a representative anisotropic diffusion method using three quantitative task-relevant metrics calculated on simulated PET images with lesions in the lung and liver. The contrast gain and noise ratio metrics were used to measure the ability to do accurate quantitation; the Channelized Hotelling Observer lesion detectability index was used to quantify lesion detectability. The adaptive filter improved the signal-to-noise ratio by more than 45% and lesion detectability by more than 55% over the Gaussian filter while producing "natural" looking images and consistent image quality across different anatomical regions.

Keywords: Image Quality, Restoration and Deblurring, Nuclear Medicine

1. INTRODUCTION

Positron emission tomography images inherently have significant levels of noise due to the limited number of photons that are detected.[1] To reduce the noise, Gaussian smoothing is commonly performed after image reconstruction. The advantage of using such a linear filter is that it has a simple implementation. However, while it smoothes noise, it also blurs edges, compromising lesion detectability and quantitation.

In order to preserve edges and smooth noise, edge-preserving smoothing algorithms can be used. Typical edge preserving filters[2, 3] estimate edge strength and accordingly adjust the amount of filtration. However, these filters assume that the noise properties are constant throughout the image. This assumption is invalid for PET images, where the noise is spatially variant, approximately following Poisson statistics. That is, the absolute noise levels in the image vary as a function of local activity concentration. For example, the noise in the liver is more than the noise in the lungs since the mean activity in the liver is greater. Therefore, a detectable edge in the liver must be stronger than a detectable edge in the lungs. Consequently, depending on the parameters, the liver will be under-smoothed or the lungs over-smoothed. To address this shortcoming, we designed an adaptive filter that adjusts the sensitivity to features based on a local estimate of the image noise.

In evaluating these algorithms, quantitative image quality metrics were used to measure and compare filtered simulated PET images having lung and liver lesions of various sizes and source-to-background ratios.

Section 2 gives an overview of the various filters used in this study. Section 3 discusses the phantom simulations and image quality metrics used to evaluate the filters. Section 4 gives the results of the evaluation, and Section 5 discusses the conclusions.

Further author information: (Send correspondence to Dirk Ryan Padfield)
Dirk Ryan Padfield: E-mail: padfield@research.ge.com
Ravi Manjeshwar: E-mail: manjeshw@crd.ge.com

2. FILTER DESCRIPTIONS

It is generally desirable to smooth the homogeneous regions of an image with two aims in mind: noise elimination and edge preservation. In addition, for PET images, the filter should be robust to noise spikes and should be able to accommodate spatially varying noise levels. The following descriptions explain the features of several filters with respect to these aims.

2.1. Gaussian Filter

Gaussian low-pass filtering computes a weighted average of pixel values in a neighborhood, in which the weights decrease as a Gaussian function with distance from the neighborhood center. Because of its simplicity and qualities such as symmetry, separability, and smooth frequency response, Gaussian filtering is used extensively for image denoising. One of its main disadvantages, however, is that it also blurs edges (compare Figures 3(a) and (b)).

2.2. Anisotropic Diffusion Filter

Anisotropic Diffusion (AD), introduced by Perona and Malik,[2] prefers intra-region smoothing over inter-region smoothing through the use of a diffusion coefficient that varies spatially. In this scheme, edges are measured by high gradient magnitude, and the conductance across the edge can be varied to limit the smoothing at the edges in the image. The basic idea is that if the gradient is large, then the diffusion will be low, and if the gradient is small, diffusion will be high.

The conduction coefficients are weights that determine the influence of a neighboring pixel on the center pixel. These coefficients are calculated using a function g that is monotonically decreasing, non-negative with $g(0) = 1$. Many choices for this function exist, but the most common choice[2] is given by

$$g\left(\nabla_X I^t_{i,j}\right) = \exp\left(-\left(\frac{|\nabla_X I^t_{i,j}|}{W_{i,j} \times K}\right)^2\right). \tag{1}$$

Another choice that uses a smoothed version of the image[3,4] is given by

$$g\left(\nabla_X I^t_{i,j}\right) = \exp\left(-\left(\frac{|\nabla_X (G_\sigma * I)^t_{i,j}|}{W_{i,j} \times K}\right)^2\right). \tag{2}$$

Here $G_\sigma * I$ is the Gaussian smoothed version of the image, which helps to remove noise spikes in the gradient estimate. The variable K in this equation is called the *conductance term*, and it determines the width of the smoothing function. For a given gradient magnitude, an increasing K results in greater smoothing. The variable W is some estimate of image gradients, like the average gradient magnitude squared, which is often included to normalize the image gradients; it is generally constant across the image. ∇_X indicates the difference between the center pixel and each of its neighbors.

The AD filter is effective for images with high signal-to-noise ratios and constant noise power throughout the image. However, if the signal is very noisy, AD can actually enhance the noise (see Figure 3(c)). It also does not support spatially varying noise power because the conductance weight W is constant across the image. In the case of PET images, these characteristics become important since the noise level scales with the local mean intensity.

2.3. Adaptive Conductance Anisotropic Diffusion Filter

As mentioned above, the AD filter assumes the image noise to be constant across the image. However, in the case of PET images, these assumptions do not hold because the noise level scales with local mean intensity. We therefore propose a method for weighting the conductance parameter of the AD algorithm adaptively across the image, based on an estimate of the local image noise. We propose two images estimates: the local median and the grayscale opening of the image.

The first image estimate is based on the median of the image using a given kernel size. A median image filter[5] computes the value of each output pixel as the statistical median of the neighborhood of values around the corresponding input pixel. It preserves edges and is effective at removing gray-level outliers, which is helpful if we view lesion pixels as gray-level outliers. Thus if the size of the neighborhood is large enough, a lesion can be completely removed, which is desirable for finding an image noise estimate. The kernel size essentially determines what size structure can be removed by the filtering.

Following the Poisson-like noise model, we estimate the image noise from the square-root of this filtered image by modifying the weight W given in equation 2. Therefore, the new weight is

$$W = \sqrt{med(I)}. \tag{3}$$

While median filtering is effective for finding an estimate of the image noise, it is computationally intensive, especially for large $3D$ neighborhoods. It also requires sorting and is not separable. A faster method is the grayscale opening of the image. The opening of an image I by a structuring element B is defined as

$$I \circ B = (I \ominus B) \oplus B, \tag{4}$$

which is the erosion of I by B followed by the dilation of the result by B,[6] where a circular kernel is used for B. If the kernel radius of the opening is of sufficient size, small local maxima are eroded while the edges of anatomical structures are retained. It has a similar effect to median filtering the image,[5] but it can be calculated much more quickly since the structuring element can be decomposed into smaller elements. The result has relatively uniform intensity throughout each structure, ignoring noise and lesions, and has distinct edges.

The new weight for the algorithm using the opened image is

$$W = \sqrt{(I \circ B)}. \tag{5}$$

Note that when using either the median or the opening methods the conductance weight is now a matrix of the same size as the original image that specifies a different amount of smoothing for each pixel, whereas previously it was constant across the image. See Figures 3(d) and 3(e) for examples of the impact of this filter.

3. METHODS

Simulated PET images were used to quantitatively compare the different filters as a function of lesion source-to-background ratio (SBR), lesion size, and count statistics. The quantitative evaluation of image processing algorithms is difficult with clinical images since 1) ground truth is not known and 2) a large number of clinical datasets are required to draw statistically meaningful results. Simulated images address both these problems by providing a large number of images with known ground truth and controllable image characteristics.

3.1. Simulations

An analytical PET system simulator was used to simulate the acquisition of the digital Zubal phantom on the GE Discovery LS PET/CT scanner operating in 2D mode. The Zubal phantom is built from a segmented CT image of a male human.[7] A spherical lesion was inserted in the lung and liver. Lesion sizes of 10, 20 and 30 mm with SBRs of 3:1, 6:1 and 9:1 were studied.

Images of size (128, 128, 105) pixels and spacing (4.29, 4.29, 4.25) mm/pixel were reconstructed with an iterative reconstruction algorithm after correcting for scatter and attenuation. For each combination of lesion size and SBR, 100 sample image sets were generated. In addition, 100 sample image sets were generated without lesions. Each of these image sets was filtered with the standard linear Gaussian filter and the edge preserving filters implemented in 3D. Several views of the phantom generated with lesion size 20 mm and SBR 3:1 can be seen in Figure 1. Figure 2 shows a cropped image section of the lung lesion along with a cropped image section of the average of all 100 samples. This theoretical average image gives a noiseless view of the phantom and is considered theoretical because a similar image for a patient would require averaging 100 scans.

3.2. Quantitative Image Quality Metrics

Clinical PET imaging tasks can be broadly classified as either detectability or quantitation tasks. We compared the different filters through three metrics relevant to these tasks: Contrast Gain, Noise Ratio, and Lesion Detectability Improvement.

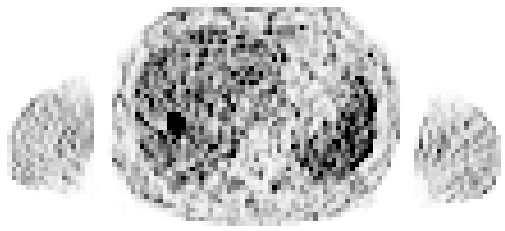

(a) Phantom Transverse Liver

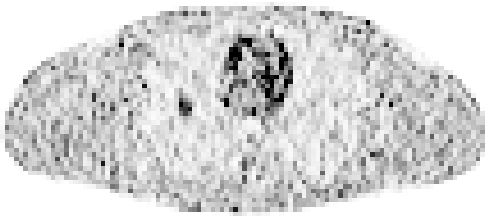

(b) Phantom Transverse Lung

(c) Phantom Coronal

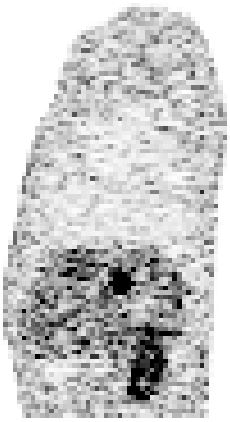

(d) Phantom Sagittal

Figure 1. Four views of the Zubal Phantom. The phantom has two 20 mm lesions with 6:1 SBR; one in the liver and one in the lung.

3.2.1. Contrast Gain

The Contrast Gain (CG) metric measures the dilution of the lesion contrast owing to the post-processing filters. Lesion contrast and contrast gain are given, respectively, by

$$C = \mu_{lesion} - \mu_{bkg} \tag{6}$$

$$CG = C_{filtered}/C_{unfiltered} \tag{7}$$

where $\mu_{filtered}$ and μ_{bkg} are the mean intensities inside a region-of-interest (ROI) centered on the lesion location for lesion-present and lesion-not-present images, respectively. $C_{filtered}$ and $C_{unfiltered}$ are the contrasts for the filtered and unfiltered images, respectively. Ideally, the filter should faithfully retain the lesion contrast while reducing the noise resulting in a CG of unity.

3.2.2. Noise Ratio

The Noise Ratio (NR) metric represents the amount by which noise is reduced through the filtering process. It is given by

$$NR = \sigma_{filtered}/\sigma_{unfiltered} \tag{8}$$

where $\sigma_{filtered}$ and $\sigma_{unfiltered}$ are the standard deviations of the pixel intensities inside an ROI centered on the background for the filtered and unfiltered images, respectively. A filter should yield as low NR value as possible, indicating that the filtered image has less noise.

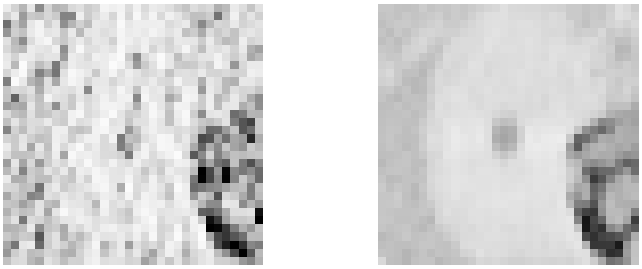

(a) Lung Image Sample (b) Lung Image Average of 100 samples

Figure 2. Examples of unfiltered lung sample and average unfiltered lung sample. The image in (a) is one sample of a cropped section of an unfiltered image. The image in (b) is the average of the 100 samples of the same cropped section. The lesion size is 20 mm, and the SBR is 3:1.

3.2.3. Lesion Detectability Improvement

The Channelized Hotelling Observer (CHO) Lesion Detectability Improvement (LDI) model has been shown to correlate well with human observer performance for the task of detection of low contrast targets in noisy images.[8] The CHO is a sub-optimal matched filter that pre-processes the input image with a bank of spatial frequency channels to extract a small number of image features. The filter bank has a physiological basis in the frequency selective response of the human visual system.[9] The lesion detectability decision statistic λ for the CHO model is given by

$$\lambda = \omega^T g \tag{9}$$

where g is the vector of image pixel values and ω is a matched filter template. The CHO matched filter template is calculated from the inverse of the covariance matrix of the channel responses. The λ values were computed for the lesion-present and lesion-not-present image sets and the detectability index, d' was computed as

$$d' = \frac{\bar{\lambda}_s - \bar{\lambda}_n}{\sigma_{\lambda_n}} \tag{10}$$

where $\bar{\lambda}_s$ and $\bar{\lambda}_n$ are the mean CHO responses to the set of lesion-present and lesion-not-present images, respectively. σ_{λ_n} is the standard deviation of the CHO response to the lesion-not-present images.

A CHO with 4 rectangular non-overlapping channels with pass bands of [0.03–0.06], [0.06–0.12], [0.12–0.25], and [0.25–0.50] cycles per pixel were used to compute d' for the filtered and unfiltered images. The d' for the filtered images were normalized by that of the unfiltered images as a metric of improvement in lesion detectability (LDI). A value $LDI = 1$ represents no improvement in lesion detection, while $LDI < 1$ and $LDI > 1$ represents lesion detection degradation and improvement, respectively.

4. RESULTS & DISCUSSION

The results of the phantom experiments for the lung and liver lesions, averaged across lesion size and SBR are given in Table 1. In this table, all values are normalized by the unfiltered values, so that values close to unity mean little change from the unfiltered images. The 10 mm lesion images with SBR of 3:1 were excluded from our analysis because this size lesion was not visible due to partial voluming effects. For comparison purposes, the parameters for the edge-preserving smoothing filters were chosen so as to result in approximately the same CG for the lung lesions as obtained from a commonly used setting of the Gaussian filter ($\sigma_s = 2.68$ mm). Equation 1 was used for the AD results, and Equation 2 with the weight in Equation 3 or 5 were used for the adaptive results.

As expected, all the image quality metric values are similar across the lung and liver lesions for the linear Gaussian filter. It is interesting to note that Gaussian filtering does not improve lesion detectability compared to the unfiltered images. Similar results have been reported for digital x-ray fluoroscopy images.[10]

For the AD filter, the CG values differ across the lung and liver lesions. This implies that the liver and lung anatomies have been filtered differently and have different point-spread functions. This is not surprising considering this filter assumes

Table 1. Summary of image quality metrics for lung and liver lesions. The parameters of each filter were chosen so as to yield approximately the same CG as the standard Gaussian filter. All values are normalized by the unfiltered values, so that values close to unity mean little change from the unfiltered images. The adaptive filter yields the lowest NR and highest LDI values.

Filter	CG		NR		LDI	
	Lung	Liver	Lung	Liver	Lung	Liver
Gaussian	0.82	0.82	0.55	0.53	1.04	1.00
AD	0.82	0.98	0.30	0.49	1.49	1.32
Adaptive median	0.77	0.83	0.29	0.26	1.57	1.56
Adaptive opening	0.80	0.84	0.30	0.26	1.57	1.56

that the noise model is uniform throughout the image. The results show that the adaptive filter adapts the filter strength depending on the local image statistics and produces consistent results across the liver and the lung lesions and produces a signal-to-noise ratio improvement of approximately 45% and a lesion detectability improvement of approximately 55% over the Gaussian. The adaptive filter yields roughly the same results for both methods of median and opening.

Filtered sample images of the liver and lung lesions are shown in Figure 3. The AD filter produces unnatural looking images with isolated noise spikes. The adaptive filter introduces no artifacts and retains the natural look of the images.

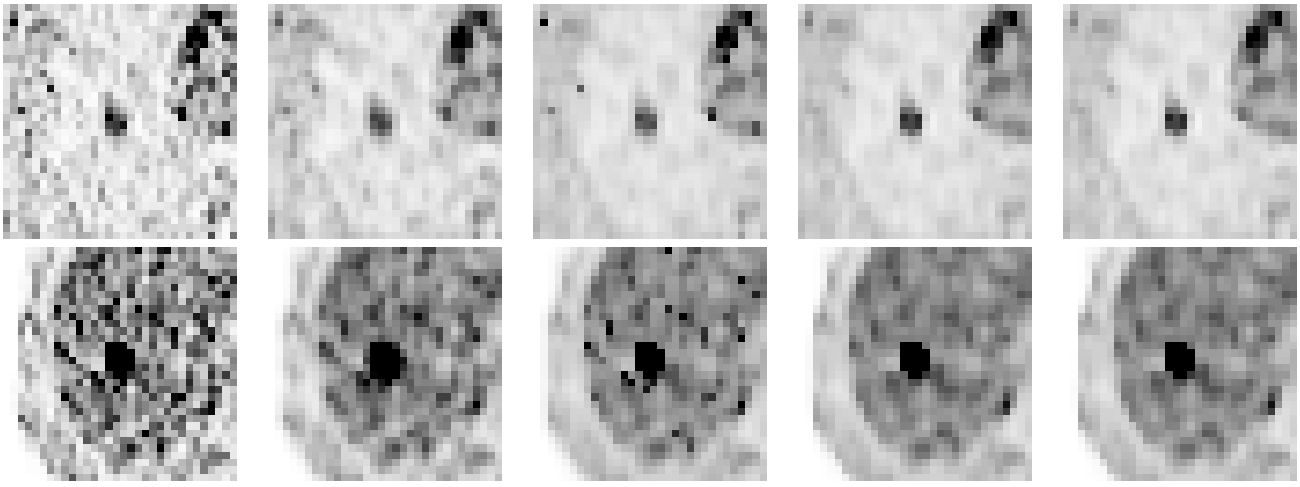

(a) (b) (c) (d) (e)

Figure 3. Zubal phantom images of the lung (top row) and liver (bottom row) regions with a 20 mm lesion with 6:1 SBR. (a) original unfiltered image, (b) Gaussian, (c) anisotropic diffusion, (d) adaptive median, and (e) adaptive opening filtered images. Only a 32 x 32 image region centered on the lesion is shown.

Figure 4 shows transverse and coronal slices of a clinical image filtered with the Gaussian filter and the adaptive filter using the opening method. The adaptive filter using the median method gives roughly the same results, so it was not included. Note that the adaptive filter smoothes the noise more effectively while retaining lesion contrast.

5. CONCLUSIONS

We presented an adaptive edge-preserving smoothing filter for smoothing PET images and evaluated its effectiveness using a combination of quantitative image quality metrics for measuring the detectability of lesions. While the AD filter offers enhanced lesion detectability compared to the standard Gaussian filter, it does not adapt to the varying noise across the image and enhances noise spikes. The new adaptive filter introduced in this paper is able to filter more consistently across structures by using an estimate of the image noise to weight the conductance parameter. We evaluated the method using two noise estimates, and other noise estimates such as pixel-wise noise variance maps could be used. Also, since this

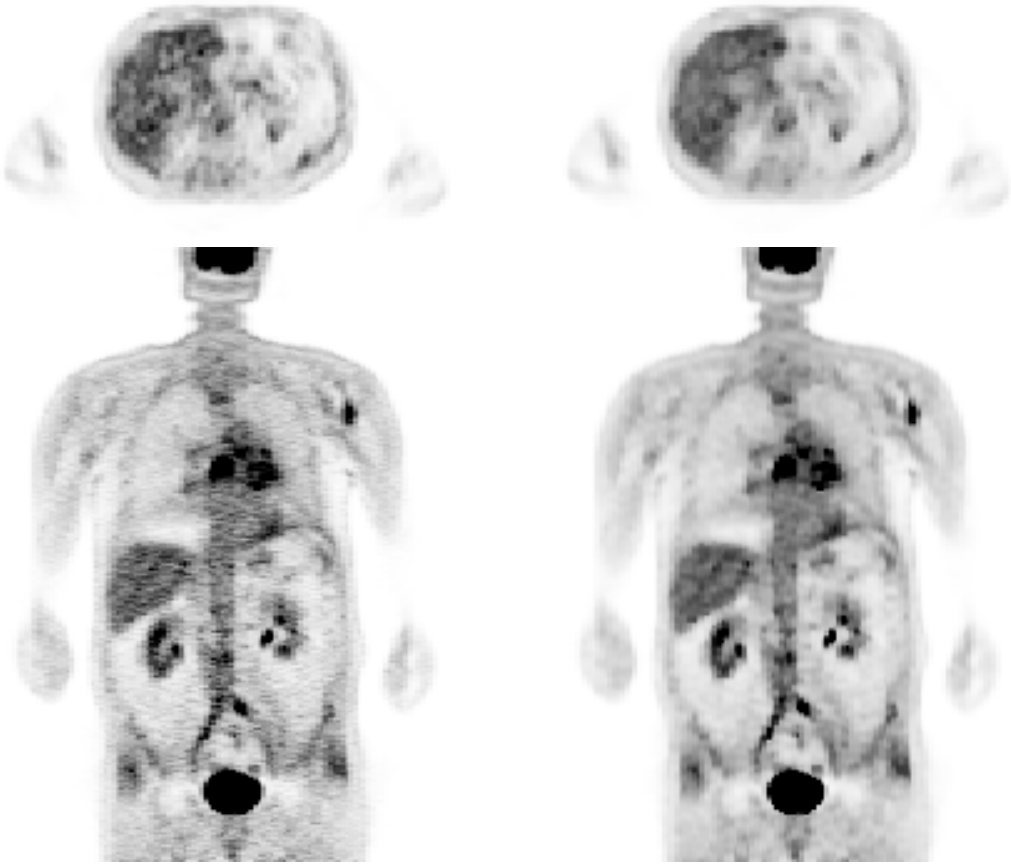

(a) (b)

Figure 4. Sample clinical image. Result of (a) Gaussian filter and (b) adaptive filter using opening method. (Clinical data courtesy of The Mayo Clinic, Rochester, MN)

framework was developed based on the Poisson-like noise characteristics of PET images, it is applicable to other images exhibiting Poisson or Poisson-like noise characteristics. We conclude that the adaptive filter has significant advantages over the Gaussian filter for smoothing PET images since it offers images with better signal-to-noise values by more than 45% and higher lesion detectability by more than 55% while maintaining the natural look of the image.

REFERENCES

1. J. A. Sorenson and M. E. Phelps, *Physics in Nuclear Medicine*, W. B. Saunders Company, 2nd ed., 1987.
2. P. Perona and J. Malik, "Scale-space and edge detection using anisotropic diffusion," *IEEE Trans. on Pattern Analysis and Machine Intelligence* **12**(7), pp. 629–639, 1990.
3. F. Catte, P. Lions, M. Morel, and T. Coll, "Image selective smoothing and edge detection by nonlinear diffusion," *SIAM J. Numer. Anal.* **29**, pp. 182–193, 1992.
4. L. Alvarez, P.-L. Lions, and J-M.Morel, "Image selective smoothing and edge detection by nonlinear diffusion (ii)," *SIAM J. on Numerical Analysis* **29**(3), pp. 845–866, 1992.
5. M. Gabbouj, E. J. Coyle, and J. N. C. Gallagher, "An overview of median and stack filtering," *Circuits, Systems, Signal Process.* **11**(1), pp. 7–46, 1992.
6. R. C. Gonzalez and R. E. Woods, *Digital Image Processing*, Addison-Wesley Publishing Company, Inc., 1992.
7. I. Zubal, C. Harrell, E. Smith, Z. Rattner, G. Gindi, and P. Hoffer, "Computerized 3-dimensional segmented human anatomy," *Medical Physics* **21**, pp. 299–302, Feb 1994.

8. K. J. Myers and H. H. Barrett, "Addition of a channel mechanism to the ideal-observer model," *Journal of the Optical Society of America* **4**, pp. 2447–57, December 1987.
9. A. Burgess, "From light to optic nerve: optimization of the front end of visual systems," *Proceedings of the SPIE: Image Perception, Harold L. Kundel, Editor* **3340**, pp. 2–13, 1998.
10. K. Jabri and D. Wilson, "Detection improvement in spatially filtered x-ray fluoroscopy image sequences," *Journal of the Optical Society of America* **3**, pp. 742–749, December 1999.